Original article

Institution of MECHANICAL ENGINEERS
Journal of AEROSPACE ENGINEERING

Proc IMechE Part G:
J Aerospace Engineering
2023, Vol. 0(0) 1–14

DOI: 10.1177/09544100231201553
journals.sagepub.com/home/pig
Sage

Optimal leading-edge deflection for flapping airfoil propulsion

Emanuel A.R. Camacho[1,2], André R.R. Silva[1] and Flávio D. Marques[2]

Abstract

The aerodynamics of oscillating airfoils are crucial to understanding subjects such as rotor dynamics and bio-inspired flows. Unsteady airfoils have been studied extensively, but there is an overall lack of knowledge regarding newer and more complex kinematics. The present paper builds upon our modified version of the NACA0012 by numerically comparing its way of flapping with the standard flapping that is common in the literature. The comparison is conducted parametrically at a Reynolds number of 10^4 for two nondimensional amplitudes. Then, using a gradient-based optimization method, we search for pitching amplitudes that maximize the propulsive power and efficiency for both flapping modes. Results indicate that the proposed flapping methodology is more promising than conventional flapping, with thrust increases up to approximately 40%. Furthermore, the proposed mechanism achieves maximum propulsive power with near-optimal efficiency, a common limitation of traditional flapping airfoils.

Keywords

Flapping airfoil, dynamic curvature, propulsive enhancement, flow control, optimization

Date received: 8 May 2023; accepted: 8 August 2023

Introduction

Birds and insects fly in a low Reynolds environment combined with an unsteady flow regime offering highly adaptive and maneuverable propulsive systems.[1] Hence, studying the aerodynamics of such systems can provide valuable insights regarding flapping-based propulsion. Furthermore, when looking at larger length and velocity scales, oscillating airfoils are central to investigating several topics, for instance, rotor blade aerodynamics and aeroelasticity. Earlier explanations of flapping wing propulsion focused on the kinematics, saying that the presence of an effective angle of attack created an aerodynamic force that had thrust and lift components.[2,3] These were expanded later on by von Kármán and Burgers,[4] who observed the change in momentum at the airfoil's wake.

The study of flapping airfoils encircles many subtopics, with most studies focusing on 2D rigid airfoils and their propulsive performance.[5] Regarding kinematics, flapping (plunging and pitching combined) is the most studied, while plunging airfoils are understudied. However, regardless of the oscillation mode, conventional airfoils have a known difficulty in offering high thrust with good efficiency, typically sacrificing one for another.[6] Thus, there is a need to discover newer geometries and innovative kinematics to improve the propulsive performance of flapping airfoils. This is a clear requirement to understand and exploit the natural flight aerodynamics, which goes beyond rigid structures with a low number of degrees of freedom and standard kinematics such as the widely used sinusoidal motion.

One of the possible geometric changes is the modification of the leading-edge geometry and its kinematics. This has been a common practice when the objective is to increase lift[7] and delay dynamic stall.[8] With that goal, Meseguer et al.[9] proposed a bio-inspired solution to improve lift using an alula-like structure. This structure resembles a leading-edge slat which improves the aerodynamic performance, particularly at higher angles of attack.[10] Likewise, Perry and Mueller[11] modified a Wortmann FX63-137 airfoil with a movable leading and trailing edge, noticeably improving lift. Other techniques, such as rotating cylinders placed at the leading edge, have

[1] Departamento de Ciências Aeroespaciais, Universidade da Beira Interior, Covilhã, Portugal
[2] Department Mechanical Engineering, Universidade de São Paulo, São Carlos, Brazil

Corresponding author:
Emanuel A.R. Camacho, Departamento de Ciências Aeroespaciais, Universidade da Beira Interior, Calçada Fonte do Lameiro, Covilhã 6201-001, Portugal.
Email: emanuel.camacho@ubi.pt

been proposed to be an effective way to prevent flow separation.[12] Others, such as Niu et al.,[13] improved the aerodynamic characteristics of a pitching NACA0012 airfoil with the variable droop leading-edge concept, verifying drag reduction and lift increase. More recent concepts, for instance, bio-inspired leading-edge serrations, have also been proven to boost aerodynamic performance.[14]

However, the use of these devices transiently is not widely explored in the literature. On top of that, studies that apply these leading-edge devices to improve the propulsive capabilities of flapping airfoils are rare. Jaworski[15] considered this problem and extended the classical theories of both Theodorsen and Garrick[16,17] to include an additional degree of freedom of a leading-edge flap and its influence on plunging and pitching.

Geissler and van der Wall[18] were one of whom studied the influence of a dynamic leading edge on propulsive performance. At a Reynolds number of 10^6, the time-dependent leading-edge deformation mitigated dynamic stall, improving thrust substantially. However, the authors recommended that experiments at lower Reynolds numbers should be conducted. In our previous work,[19] we modified the conventional NACA0012 airfoil by adding a deflectable leading edge to be used at the lower spectrum of the Reynolds number. The geometry was subjected to a parametric study[20] which exposed the tremendous potential of a movable leading edge to improve the overall propulsive performance of unsteady airfoils.

Nonetheless, the usage of unsteady airfoils or flow-control devices in an optimal manner is not common, which can lead to the underestimation of these systems' real potential. One way to tackle this is to use optimization algorithms as Tuncer and Kaya[21] did. The study was focused on finding plunging and pitching amplitudes and phase shifts between these that could maximize thrust. Results show that when thrust is maximized, propulsive efficiency is affected negatively. The same was verified by Kaya and Tuncer,[22] who optimized thrust by finding the parameters of a nonuniform rational B-spline that governed the airfoil kinematics.

Yu et al.[23] focused on three NACA 4-digit airfoils with different thicknesses. Using a gradient-based optimization algorithm, they found out that maximum propulsive efficiency is higher on thinner airfoils which can offer more than 50% when the oscillating kinematics are optimized. Focused only on optimizing pitching kinematics, Culbreth et al.[24] concluded that it is crucial to delay the onset of leading-edge separation, which is found to maximize propulsive efficiency.

The flapping motion of a NACA0012 was studied by Soueid et al.,[25] who used sensitivity functions as a means to find amplitudes and phase angles that could maximize the propulsive efficiency. Results show that a constant maximum effective angle of attack between 10° and 12° is favorable as is a 90° phase angle between plunging and pitching motions. The same optimization variables are used by Kaya et al.[26] to find optimal thrust and propulsive efficiency for a biplane configuration. For a Strouhal number between 0.17 and 0.25, the studied configuration produces more thrust than a single airfoil. However, at higher Strouhal numbers, no advantage is seen against the single-flapping airfoil.

The objective of the present paper is to further extend our previous study[20] by comparing the usage of a pitching leading edge against standard flapping in which the whole airfoil has a pitching component. Not only that, it fills a specific void in the literature where flapping airfoils are not widely examined optimally nor are their kinematics or geometric modifications improving enough. Both flapping modes are studied parametrically and optimally using gradient-based optimization. The study is conducted at a Reynolds number of 10^4 and aims to contrast the propulsive power and efficiency of the two flapping configurations. The Reynolds number is selected based on the typical Reynolds range where insects and some birds fly.[27]

Methodology

The present work uses the so-called NACA0012-IK30 airfoil, which has been explicitly designed to study the influence of a pitching leading edge on the propulsive performance of unsteady airfoils. Figure 1 shows the proposed geometry, which is obtained by splitting the NACA0012 airfoil using a circular arc, creating a gap of 1 mm between the two parts. The leading edge and back parts will be referred to as the β and ψ parts, respectively. These are separated at 30% of the chord, which coincides with the leading-edge pivot point. The same airfoil modification is also used to study standard flapping, with the same pivot point.

Regarding kinematics, the plunging motion and pitching of the leading edge follow sinusoidal waveforms, while the back part has no pitching component or mean angle of attack. The vertical translation is given by

$$y/c = h\cos(2\pi ft), \tag{1}$$

where c is the chord, h is the nondimensional amplitude, and f is the motion frequency. The angle of attack of the leading edge is written as

$$\beta = A_\beta \cos(2\pi ft + \phi), \tag{2}$$

where A_β is the leading-edge pitching amplitude and ϕ is the phase angle, set to 90°. This angle is selected so that when the airfoil has its maximum plunging velocity, the leading edge is maximally deflected.

Both the plunging and pitching velocities are used to calculate the effective angle of attack, which is defined as

$$\alpha_{\text{eff}} = \arctan\left(-\frac{\dot{y}}{U}\right) + \alpha, \tag{3}$$

where U is the freestream velocity and α is the airfoil angle of attack and is calculated as

$$\alpha = \arctan\left(\frac{c_\beta \sin\beta}{c_\beta \cos\beta + c_\psi}\right), \tag{4}$$

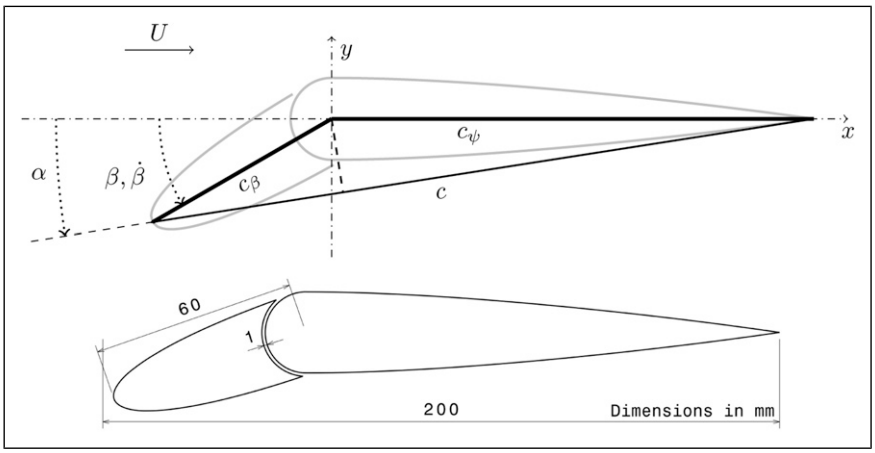

Figure 1. NACA0012-IK30 airfoil.

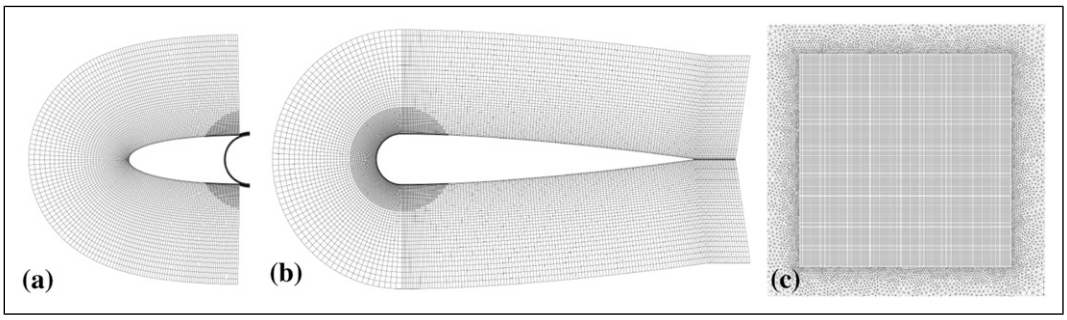

Figure 2. Leading-edge mesh (a), back-part mesh (b), and background mesh (c). Images are not to scale.

with c_β and c_ψ being the length of the frontal and back parts, respectively. The pitching amplitude of the airfoil, A_α, is determined when β equals the leading-edge pitching amplitude, A_β.

The aerodynamics of the proposed geometry is studied numerically using Ansys® Fluent. The problem is assumed to be governed by turbulent flow with laminar-to-turbulent transition. A RANS (Reynolds-Average Navier-Stokes) approach is selected to solve the problem, with the Reynolds stress tensor being modeled according to Boussinesq's hypothesis. The selected turbulence model is the SST (Shear-Stress Transport) $k-\omega$ coupled with the Intermittency Transition Model.

The governing equations are solved in a coupled manner linking momentum and pressure-based continuity equations implicitly. The Least Squares Cell-Based method is used to evaluate gradients, and the pressure interpolation is achieved with a second-order scheme. The convective terms of momentum, turbulence kinetic energy, specific dissipation rate, and intermittency equations are discretized using the second-order upwind method, while diffusive terms use a central-differenced scheme. Temporal discretization is accomplished implicitly with the first-order method.

The problem is solved using an overset mesh with two component meshes and a background mesh, as illustrated in Figure 2. This allows for higher pitching amplitudes without the challenges of deformable meshes and remeshing methods.

The NACA0012-IK30 airfoil is placed over the structured region of the background mesh and is treated with the no-slip condition. Both the inlet and outlet are placed far from the airfoil ($\approx 20c$) with a prescribed velocity and pressure, respectively. The motion of the airfoil parts and surrounding meshes are coded into User-Defined Functions (UDFs). All kinematic parameters are calculated based on the dimensionless parameters that govern the problem. These are the Reynolds number, $Re = \rho Uc/\mu$, reduced frequency, $k = 2\pi fc/U$, nondimensional amplitude, $h = A/c$, and nondimensional velocity, kh, where ρ is the fluid density, μ is the dynamic viscosity, A is the plunging amplitude, and c is the aerodynamic chord when the leading edge has no deflection.

The propulsive performance of the airfoil is monitored using the mean propulsive power, mean required power, and propulsive efficiency. In its coefficient form, the propulsive power is given by

$$C_{P_P} = (C_t)_\beta + (C_t)_\psi, \tag{5}$$

which has the same value as the thrust coefficient. The power required to sustain the airfoil motion is expressed by the required power coefficient given by

$$C_{P_R} = -\left(((C_l)_\beta + (C_l)_\psi)\frac{\dot{y}}{U_\infty} + (C_m)_\beta \frac{\dot{\beta}c}{U_\infty}\right). \tag{6}$$

In equation (6), only the $(C_m)_\beta$ was considered since no pitching was prescribed to the ψ part. The propulsive efficiency is then calculated by

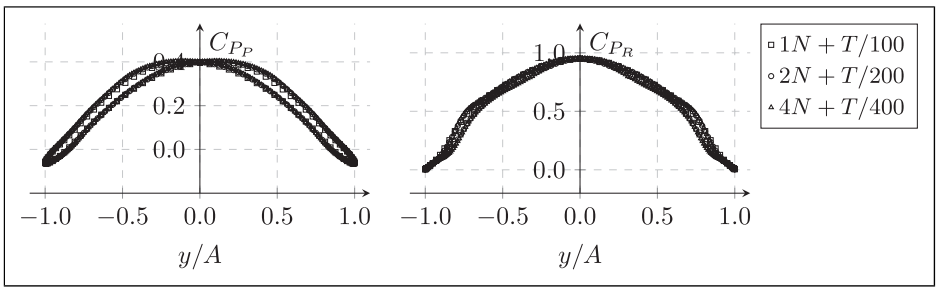

Figure 3. Mesh sensitivity analysis.

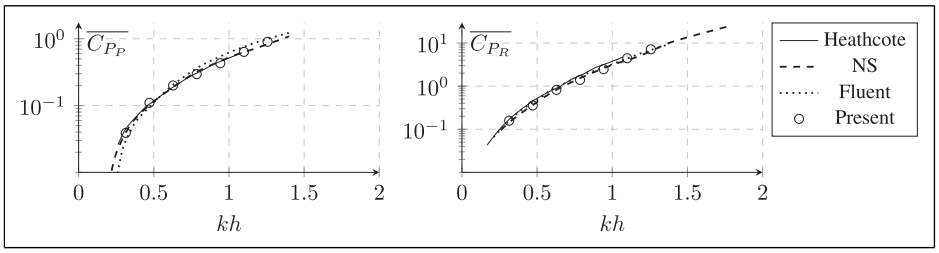

Figure 4. Numerical validation using data from Ref. 28 (NS and Fluent) and Heathcote Ref. 29.

$$\eta = \frac{\overline{C_{P_P}}}{\overline{C_{P_R}}}, \tag{7}$$

where $\overline{C_{P_P}}$ and $\overline{C_{P_R}}$ are the mean propulsive power and required power coefficients, respectively, calculated on the last period where transients were negligible. The proposed geometry is also used to study the commonly studied flapping where the whole airfoil oscillates with the same pitching amplitude, meaning that $A_\beta = A_\psi = A_\alpha$. Important to note that in this configuration, the term $(C_m)_{\dot{\psi}} \dot{\psi} c/U_\infty$ must be included in equation (6).

In Figure 3, a grid and time step sensitivity study is shown for Re = 10^4, $k = 1.0$, $h = 0.50$, and $A_\beta = 5°$. Three meshes with different time steps depending on the motion period, T, are considered with all elements close to the wall respecting the $y^+ \approx 1$ mesh requirement. The parameter N is the number of mesh elements of the coarse mesh, with the final mesh ($2N$) having around two hundred thousand elements.

No significant variations demonstrate that mesh and time step independence were attained. Additionally, to further validate the numerical methodology, the published data of a plunging NACA0012,[28] including data from Heathcote et al.,[29] is compared against the current approach, as shown in Figure 4. The accuracy of the CFD findings at such a low Reynolds state is checked using the mean propulsive and required power coefficients. The computations are performed with various non-dimensional velocities at Re = 2.0×10^4 and $h = 0.175$.

Regarding the optimization methodology, a gradient-based method is used which follows the gradient direction and leads to a desired maximum of a function. This is how the optimal pitching amplitudes were found for the present study. Mathematically, it is expressed as

$$A_\alpha^{n+1} = A_\alpha^n \pm \gamma_n \frac{\mathrm{d}F}{\mathrm{d}A_\alpha}, \tag{8}$$

where F is the objective function, γ_n is the optimization step size, n represents the current iteration, and $n + 1$ is the following one. The objective function, F, in the present work, is defined as

$$F = \varphi \overline{C_{P_P}} + (1 - \varphi)\eta, \tag{9}$$

where φ is a variable that weighs between the maximization of thrust and propulsive efficiency. The gradient of F is evaluated using a backwards-finite difference as

$$\nabla F = \frac{\mathrm{d}F}{\mathrm{d}A_\alpha} \approx \varphi \frac{\overline{C_{P_P}}^n - \overline{C_{P_P}}^{n-1}}{A_\alpha^n - A_\alpha^{n-1}} + (1 - \varphi) \frac{\eta_t^n - \eta_t^{n-1}}{A_\alpha^n - A_\alpha^{n-1}}. \tag{10}$$

The optimization step size, γ_n, uses the Barzilai-Borwein method,[30] being calculated as

$$\gamma_n = \frac{\left|\left(A_\alpha^n - A_\alpha^{n-1}\right)\left(\nabla F\left(A_\alpha^n\right) - \nabla F\left(A_\alpha^{n-1}\right)\right)\right|}{\left|\nabla F\left(A_\alpha^n\right) - \nabla F\left(A_\alpha^{n-1}\right)\right|^2}. \tag{11}$$

Additional to the user-defined function used to control the airfoil kinematics, a sequence of instructions is implemented to conduct the optimization study of the airfoil pitching amplitude. The overall procedure for the optimization starts by providing an initial guess that is communicated to ANSYS Fluent. During the simulation and at every time step, two data files (kinematics and forces report) are created, which are later used to calculate the propulsive indicators and provide a new pitching amplitude guess. The mean values are calculated using the last period simulated, and at every optimization step, these are reported in a results data file with some additional information. After each oscillation cycle, the optimization kicks in,

suggesting a new pitching amplitude depending on the objective function. A pitching amplitude is considered converged when $|A_\alpha^{n+1} - A_\alpha^n|/|A_\alpha^n|$ is kept under 1% for five consecutive periods. The optimization framework is shown in Figure 5.

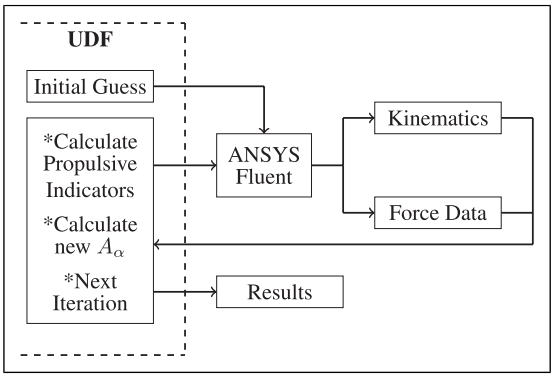

Figure 5. Optimization methodology.

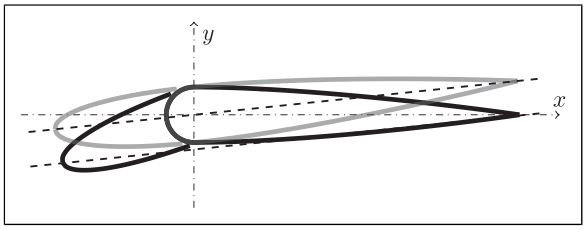

Figure 6. NACA0012-IK30 airfoil (black) *vs.* standard flapping (gray).

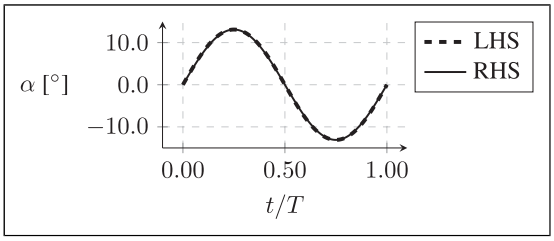

Figure 7. Validation of the comparison framework.

Results and discussion

In this study, the NACA0012-IK30 mechanism and standard flapping are compared at a Reynolds number of $Re = 10^4$ under different nondimensional amplitudes and velocities. To compare the two flapping modes, the propulsive coefficients and efficiency are used, but comparing these two flapping modes requires an adequate comparison framework. A noticeable difference is that standard flapping does not present a dynamic curvature, as the proposed mechanism has. Thus, geometrical differences are kept aside, focusing only on equalizing the effective angle of attack waveform. The geometrical solution for such a problem at a given instant is shown in Figure 6.

For standard flapping, pitching is accomplished by simply following a sinusoidal wave. Although the angle of attack of the -IK30 airfoil does not follow a sinusoidal path, as shown in equation (4), it can be approximated by a sine function as

$$\arctan\left(\frac{c_\beta \sin(A_\beta \sin(2\pi f t))}{c_\beta \cos(A_\beta \sin(2\pi f t)) + c_\psi}\right) \approx A_\alpha \sin(2\pi f t), \quad (12)$$

where A_α equals the maximum angle of attack that the -IK30 airfoil experiences during the oscillation cycle. This approximation is validated in Figure 7, where the left-hand side and right-hand side of equation (12) are plotted for a leading-edge pitching amplitude of 45°. No leading-edge pitching amplitudes surpassed 45°, making this an adequate comparison framework to analyze the two flapping modes.

The first phase of results consists of studying the two flapping modes parametrically. Two nondimensional amplitudes are considered ($h = 0.25$ and 0.50), each with three nondimensional velocities ($kh = 0.25$, 0.50, and 1.00). The leading-edge pitching amplitude of the proposed geometry is varied between 0° and 20°, resulting in a pitching amplitude between 0° and 6°. In Figure 8, the mean propulsive power coefficient is shown as a function of the pitching amplitude, with (S) representing standard flapping.

Regardless of the nondimensional amplitude, the proposed mechanism offers more propulsive power when compared to conventional flapping, except at lower nondimensional velocities. However, at the lowest nondimensional velocity, the improvements of both ways of flapping are not as considerable as the ones seen for $kh = 0.50$ and 1.00. Such occurrence is expected at slow flapping conditions, which are near

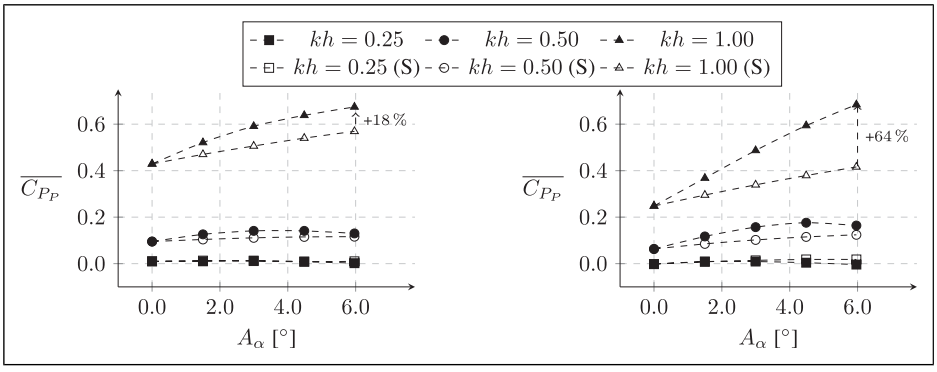

Figure 8. Mean propulsive power coefficient for $h = 0.25$ (left) and $h = 0.50$ (right). Standard flapping is represented by (S).

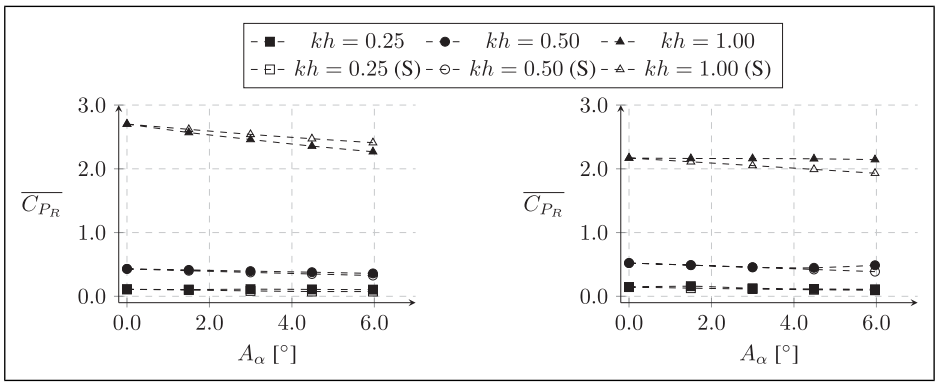

Figure 9. Mean required power coefficient for h = 0.25 (left) and h = 0.50 (right). Standard flapping is represented by (S).

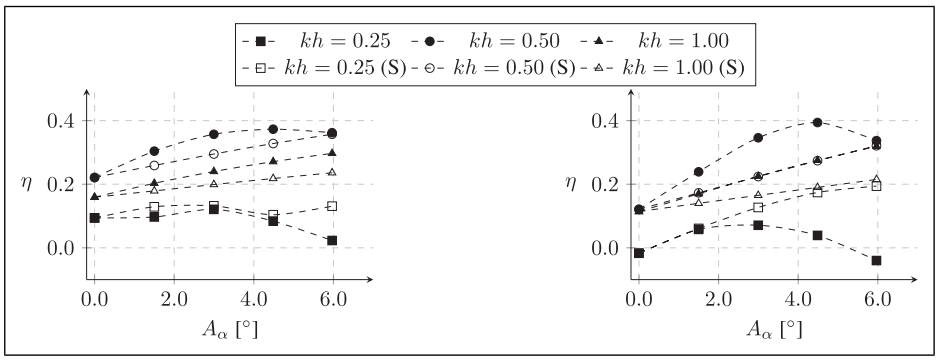

Figure 10. Propulsive efficiency for h = 0.25 (left) and h = 0.50 (right). Standard flapping is represented by (S).

drag-producing regimes. Furthermore, the improvements obtained using the proposed geometry become more significant as the nondimensional amplitude rises, offering increases of up to 64%. This last condition has a deep resemblance with bird flight, specifically the takeoff and landing phases. In these stages of flight, where lower Reynolds numbers and high nondimensional velocities are imposed, animals morph their wings into highly curved configurations, suggesting that dynamic curvature is a primary requirement for effective thrust production, which is crucial while performing evasive maneuvers.

The main difference between the two flapping modes occurs at $kh = 0.50$, where after reaching its maximum, the $\overline{C_{P_P}}$ provided by the leading-edge mechanism starts decreasing, while conventional flapping is still increasing. This is not observed at kh = 1.00, suggesting that the range of pitching amplitudes where the NACA0012-IK30 airfoil offers greater performance over conventional flapping depends not only on the pitching amplitude but also on the $k - h$ combination.

Regarding power consumption, shown in Figure 9, conventional flapping consumes less power, except when kh = 1.00 for the lowest nondimensional amplitude. Overall, regardless of the flapping method, there is less power being consumed compared to a pure plunging airfoil. This results from the lower effective angle of attack that is experienced either by deflecting just the leading edge or the whole airfoil.

Propulsive efficiency exhibits a different tendency when compared to the other propulsive indicators, as shown in Figure 10. With kh = 0.25, standard flapping is superior for both nondimensional amplitudes, although, at the lowest amplitude, it shows a dip close to A_α = 4.5°. With h = 0.50 we see two branches where traditional flapping continually increases, and the other has its efficiency quickly degraded. Nevertheless, this nondimensional velocity has limited propulsive purposes judging by the small thrust provided. Results at higher nondimensional velocities become different as the NACA0012-IK30 airfoil now offers better propulsive efficiency for the range studied. However, at $kh = 0.50$, the trends indicate that conventional flapping will surpass the -IK30 after 6°. The same is not observed at kh = 1.00, where the NACA0012-IK30 airfoil has better propulsive efficiency with no clear sign of performance degradation. However, this does not mean that at higher pitching amplitudes, it will not be surpassed by standard flapping.

This parametric study proves that having a dynamic leading-edge offers superior propulsive performance compared to conventional flapping, with the latter being the norm in most research in the literature. This suggests that the dynamic curvature induced by the leading-edge deflection is favorable at the conditions studied, meaning there is no real need to pitch the whole airfoil.

One could argue that the range considered for this parametric is small as the pitching amplitude is kept under 10°. Thus, comparing the two flapping modes is extended to higher pitching amplitudes by searching for optimal thrust and efficiency. The Reynolds number is kept at 10^4, and only the highest nondimensional amplitude, h = 0.5, is tested, although similar trends are expected

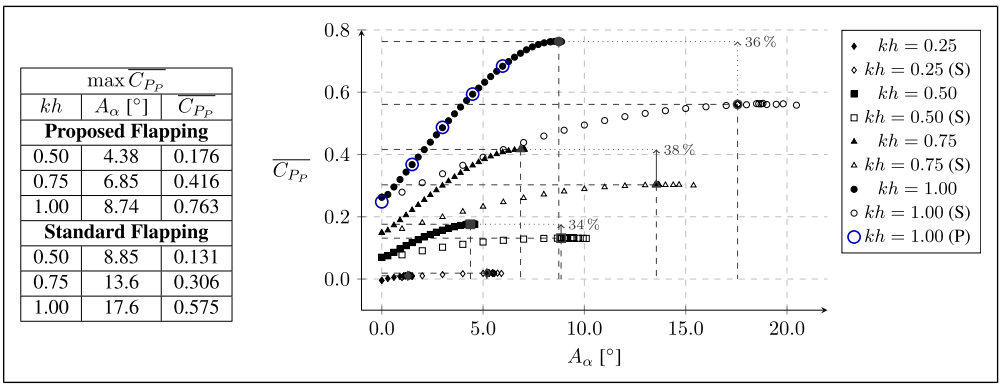

max $\overline{C_{P_P}}$		
kh	A_α [°]	$\overline{C_{P_P}}$
Proposed Flapping		
0.50	4.38	0.176
0.75	6.85	0.416
1.00	8.74	0.763
Standard Flapping		
0.50	8.85	0.131
0.75	13.6	0.306
1.00	17.6	0.575

Figure 11. $\overline{C_{P_P}}$ as a function of A_α during the optimization of the propulsive power (φ = 1.0). Standard flapping is represented by (S).

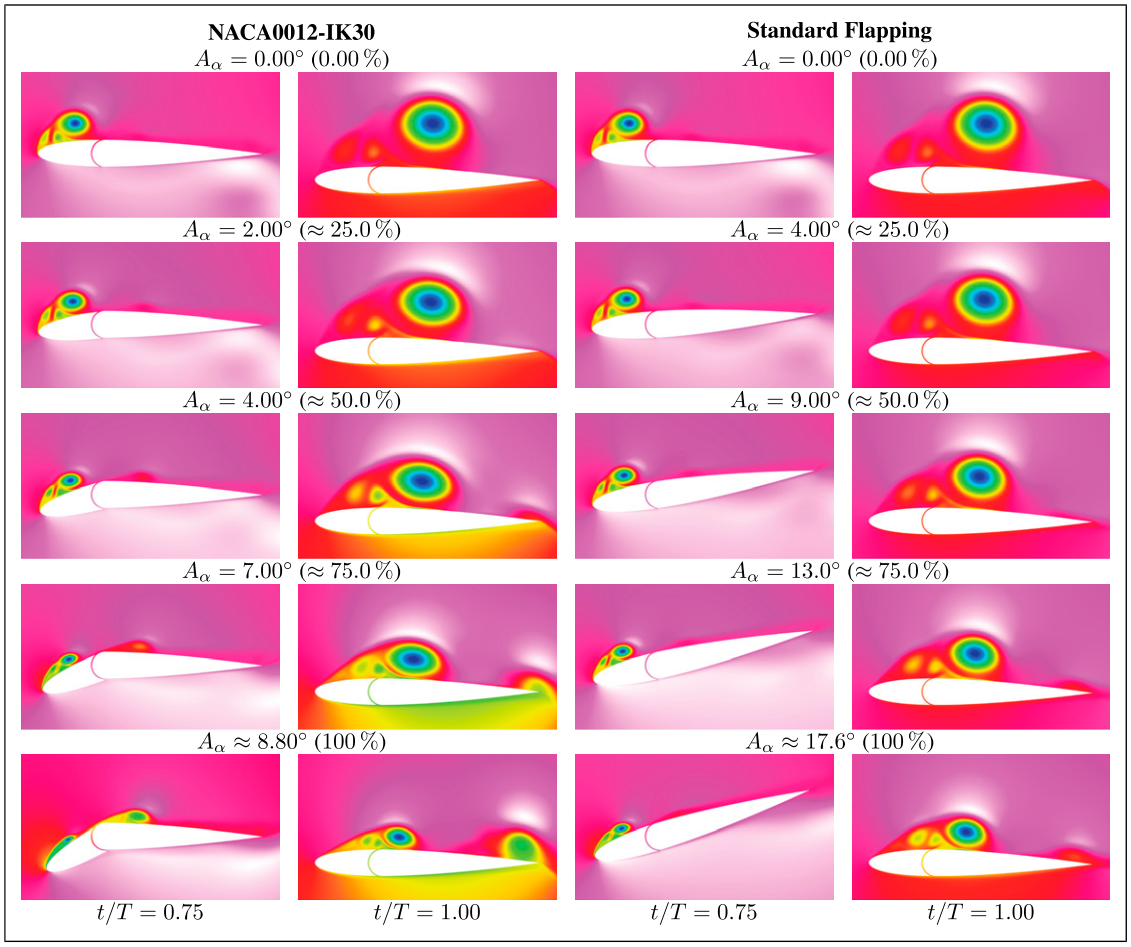

Figure 12. Optimization progress with φ = 1.0.

for a nondimensional amplitude of 0.25. An additional nondimensional velocity (kh = 0.75) is added to the comparison.

Optimization of $\overline{C_{P_P}}$

The first part of the optimization process is focused on maximizing the propulsive power, meaning that φ = 1 in equation (9). Furthermore, the change in the pitching amplitude is limited to 1°. This limiter reduces existing transients between consecutive periods, which allows for a A_α adjustment after each period. Moreover, the optimization of the -IK30 mechanism is made using the leading-edge pitching amplitude instead of the airfoil pitching amplitude.

In Figure 11, the mean propulsive power is shown as a function of the airfoil pitching amplitude, with each data point representing an iteration step. Additionally, a parametric study (P) for the highest nondimensional velocity where higher transients are expected shows that the limiter as mentioned above works appropriately.

The mean propulsive power increases with the nondimensional velocity regardless of the flapping mode. Moreover, for each kh, there is a pitching amplitude that maximizes thrust. These are global maximums since null or excessive deflection holds no real benefit. At the lowest nondimensional velocity, $kh = 0.25$, both flapping methodologies offer no significant advantage. As verified in the parametric study, this is a slow flapping condition causing the airfoil to be very close to the drag-producing regime. However, for kh greater than 0.5, the pitching amplitude influences the mean propulsive power. Results show that by only deflecting the leading edge, much higher propulsive power is achieved compared to standard flapping at the same angle of attack. Comparing peak performance, the proposed mechanism can offer an increase of up to 38% at a much lower pitching amplitude. Moreover, as kh increases, the pitching amplitude that maximizes the propulsive power also increases for both ways of flapping, though this growth is thought to be asymptotic.

To understand the thrust enhancement mechanism for the two flapping modes, we provide some snapshots of the total pressure field plus the pressure coefficient of the airfoil surface. The total pressure is only used as a qualitative parameter to identify flow-separated regions. In Figure 12, the $\overline{C_{P_P}}$ optimization process is shown for $kh = 1.00$ at two instants, $t/T = 0.75$ and $t/T = 1.00$. Other kh conditions are similar, although effects are scaled down. Analyzing the images of both flapping configurations, although having broadly different geometries, they present the same flow patterns. At the beginning of the optimization process (0.00% of max F), the flow separates right at the leading edge during the descent, creating a massive separated region at the end of the period. As the optimization process progresses, we observe that the leading-edge vortex (LEV) has its size reduced, although not being completely cleared. This indicates that the maximization of the propulsive power is accomplished by the presence of the LEV. One could expect such a result since the LEV is a low-pressure region that effectively works as a suction force in the β part. An additional result that differentiates the two modes is that the proposed flapping creates an additional vortex at the ψ part, close to the pivot point, which is enlarged as the leading-edge pitching amplitude increases. As will be seen ahead, this vortex will be the main reason why the required power increases when compared to standard flapping.

In Figure 13, five snapshots of the descending phase (the ascending phase is similar but symmetrical) are shown at maximum $\overline{C_{P_P}}$. The pressure coefficient at the airfoil surface is also provided for both standard and proposed flapping. As seen in Figure 12, the maximization of the propulsive power requires the presence of a LEV, which being a low-pressure zone, acts as a thrust booster for both flapping modes. As the airfoil accelerates downwards ($t/T = 0.625$), a suction zone appears on the frontal part of the upper surface, which has a peak right at the leading edge. Following this peak is an adverse pressure gradient that is the cause of the flow separation and subsequent LEV formation.

Furthermore, for the proposed flapping, there is an additional adverse pressure gradient appearing at the pivot point due to the dynamic curvature of the NACA0012-IK30, which results in flow separating at two different places, as captured at $t/T = 0.75$. Looking at C_P, although the suction zone at the β part is similar for both flapping modes, the ψ part of the proposed flapping presents an additional suction zone that majorly contributes to lift, leading to an increase in consumed power. As the airfoil continues its descent, these low-pressure zones are diluted until reaching the bottom position, where the pressure distribution is virtually the same for both flapping configurations.

Additional to the pressure distribution, we also present the propulsive coefficients over time to comprehend why the proposed flapping offers more thrust and what are the contributions of each airfoil part in these coefficients. In Figure 14, the C_{P_P} decomposition is provided, where we see that the leading edge is the main contributor, with the proposed geometry providing an approximate 50% increase compared to standard flapping while at peak performance. The ψ part is similar to conventional flapping, offering a slight improvement.

It is worth stopping here and questioning how the proposed flapping methodology outperforms conventional flapping in terms of thrust production. The root cause of such improvements is uncovered by revisiting the distribution of the pressure coefficient and by looking at the overall frontal area of the airfoil during the oscillation cycle (Figure 13). As one can see, while both flapping modes have similar pressure coefficient distributions, the frontal part in the proposed flapping has a larger deflection than in standard flapping. This larger deflection combined with the suction peak located at the leading edge, increases the resultant force in the streamwise direction, in this case thrust. This is how conventional flapping can be surpassed by the NACA0012-IK30 airfoil.

Contrary to C_{P_P}, the consumed power by the β part of the airfoil for both flapping configurations is nearly the same as observed in Figure 15. However, when looking at the ψ part, it is clear that standard flapping consumes considerably less power, mainly because it does not have that vortex seen in the pitching-only leading edge case that is formed at the pivot point and is responsible for a higher lift.

This is why the two flapping modes present very different power requirements at maximum propulsive power. In Figure 16, the mean propulsive power coefficient is shown as a function of the mean required power coefficient.

The -IK30 mechanism, while providing more thrust, consumes more power than standard flapping. When at peak propulsive power, the proposed geometry requires up to 36% more power than the conventional way of flapping for $kh = 1.00$. At lower nondimensional velocities, it goes down to 27% if we neglect the smallest kh.

Before moving to the optimization of propulsive efficiency, it is vital to remember that we are

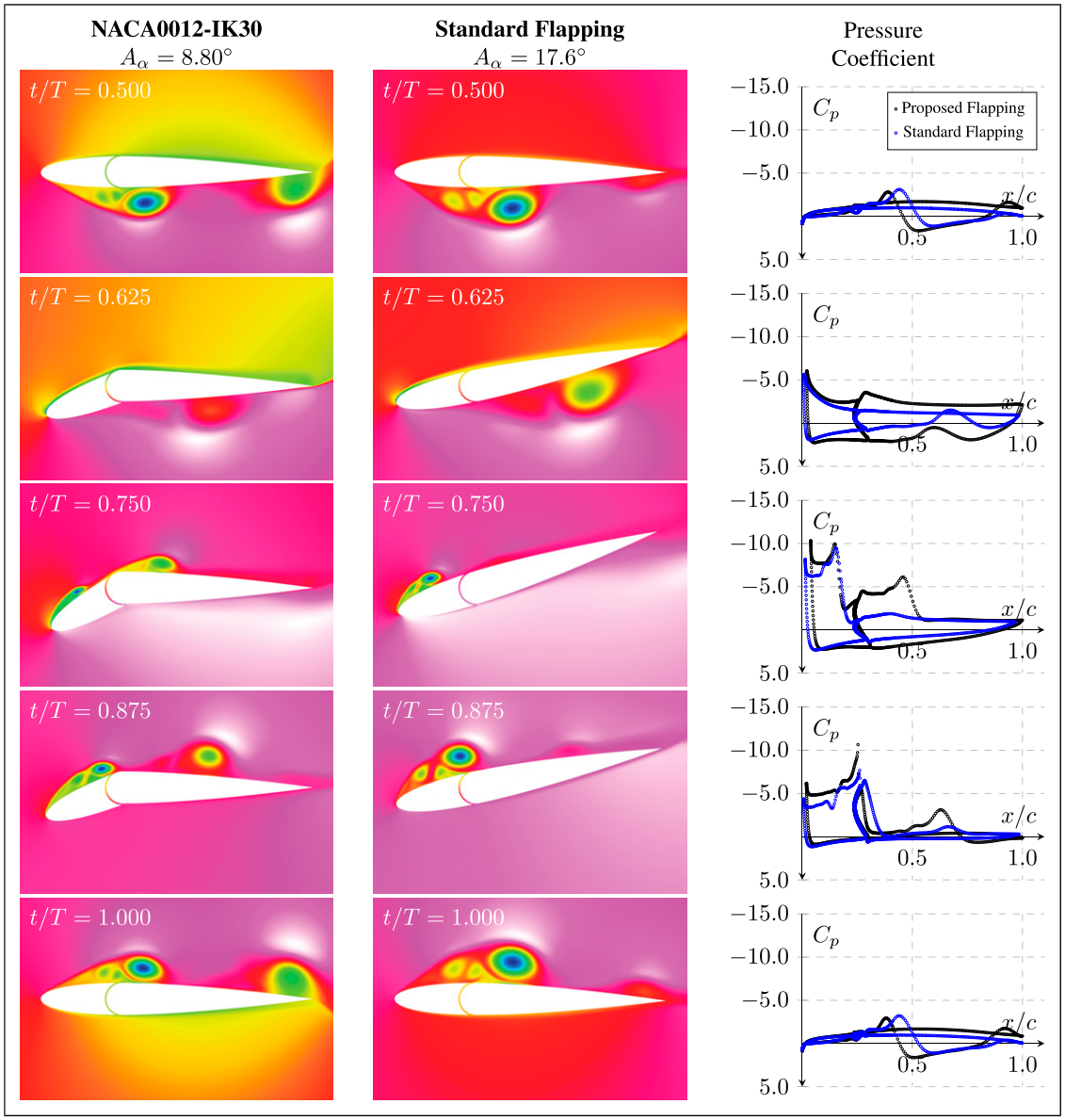

Figure 13. Pressure distribution for the two flapping modes at maximum propulsive power.

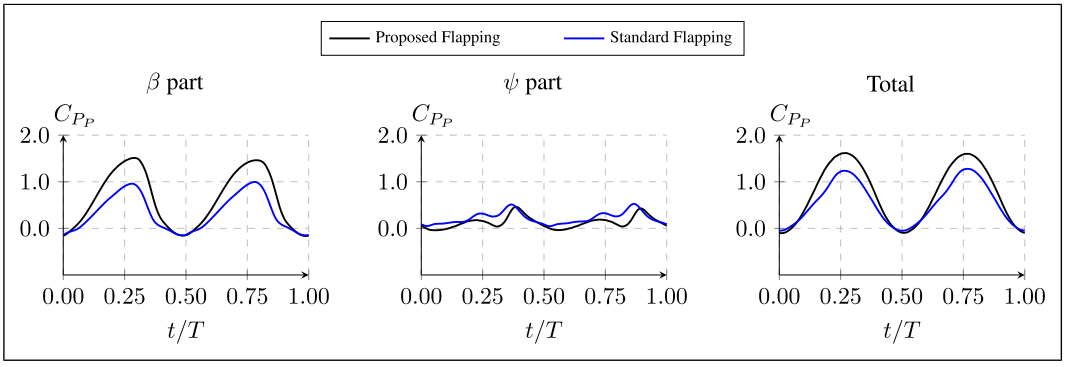

Figure 14. Propulsive power coefficient decomposition when φ = 1.0.

maximizing the propulsive power while maintaining the phase angle constant at 90°. By doing this, we are looking exclusively at the influence of the pitching amplitude, by restricting the known influence that the phase angle has on thrust production. The impact of the latter is a crucial matter for future research. However, this limitation does not interfere when we are looking for the optimization of the propulsive

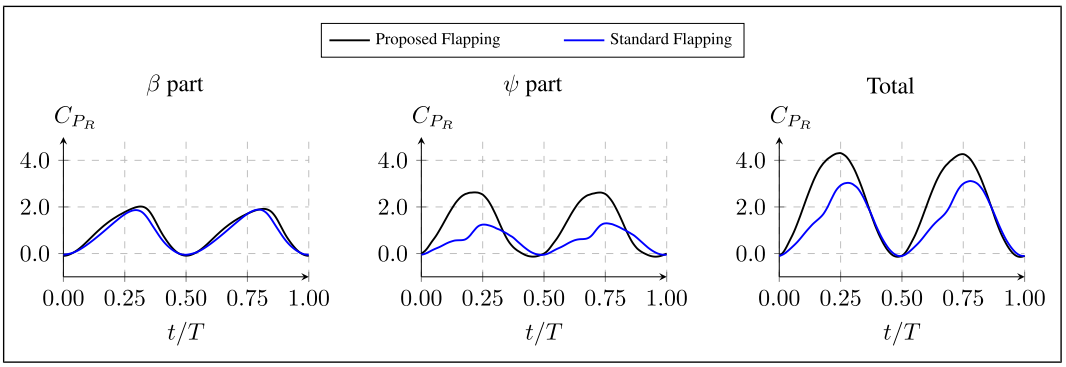

Figure 15. Required power coefficient decomposition when φ = 1.0.

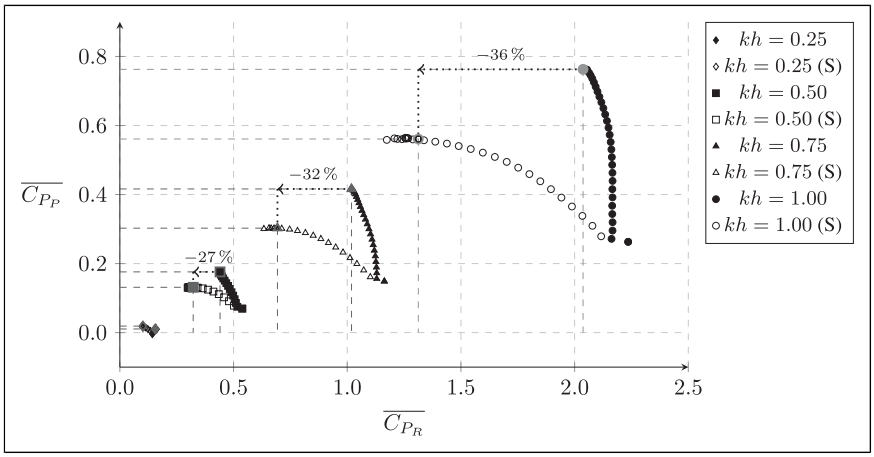

Figure 16. $\overline{C_{P_P}}$ as a function of $\overline{C_{P_R}}$ during the optimization of the propulsive power (φ = 1.0). Standard flapping is represented by (S).

max η		
kh	A_α [°]	η
Proposed Flapping		
0.50	4.37	0.399
0.75	7.39	0.409
1.00	9.60	0.375
Standard Flapping		
0.50	14.4	0.505
0.75	21.9	0.564
1.00	27.7	0.543

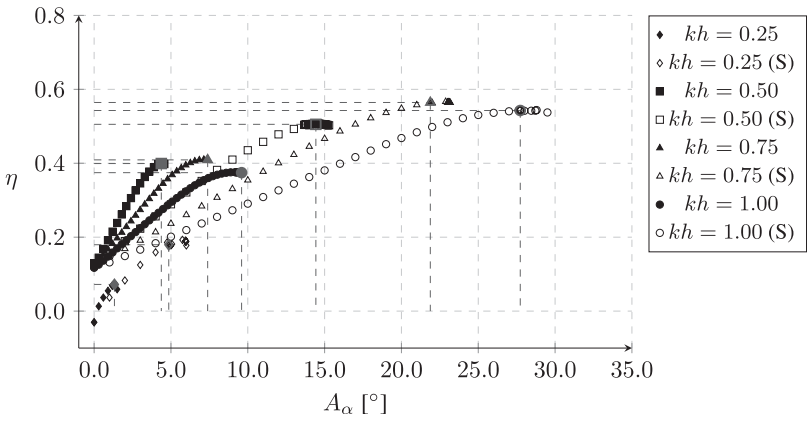

Figure 17. η as a function of A_α during the optimization of the propulsive efficiency (φ = 0.0). Standard flapping is represented by (S).

efficiency, which is known to reach its maximum when the phase angle is 90°.

Optimization of η

The optimization methodology is extended to the propulsive efficiency (φ = 0.0) in Figure 17. Higher efficiency is achieved by standard flapping mainly due to the lower power demand it requires. At kh = 0.25, efficiency is pretty low for both flapping modes, mainly due to the insignificant propulsive power generated. For other nondimensional velocities, the pitching component offers noticeable enhancements, with conventional flapping achieving propulsive efficiencies close to 60%. Maximum efficiency is achieved for kh = 0.75 regardless of flapping methodology, showing that, unlike

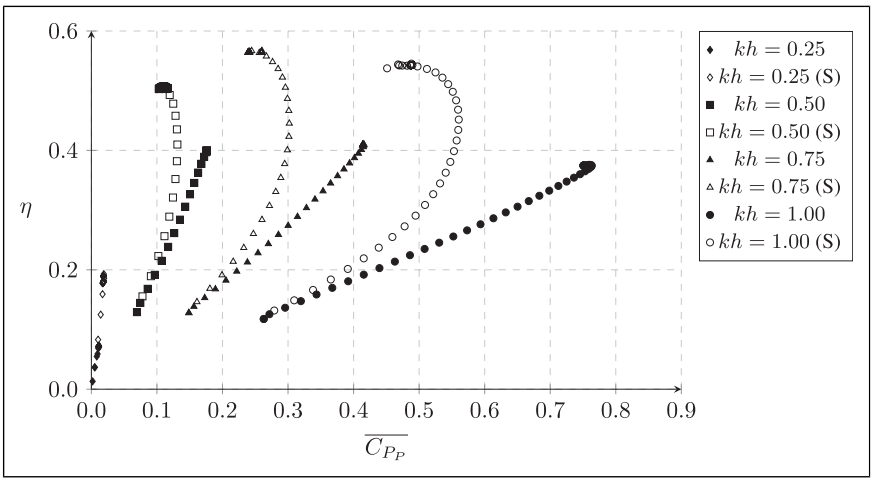

Figure 18. η as a function of CPP during the optimization of the propulsive efficiency (φ = 0.0). Standard flapping is represented by (S).

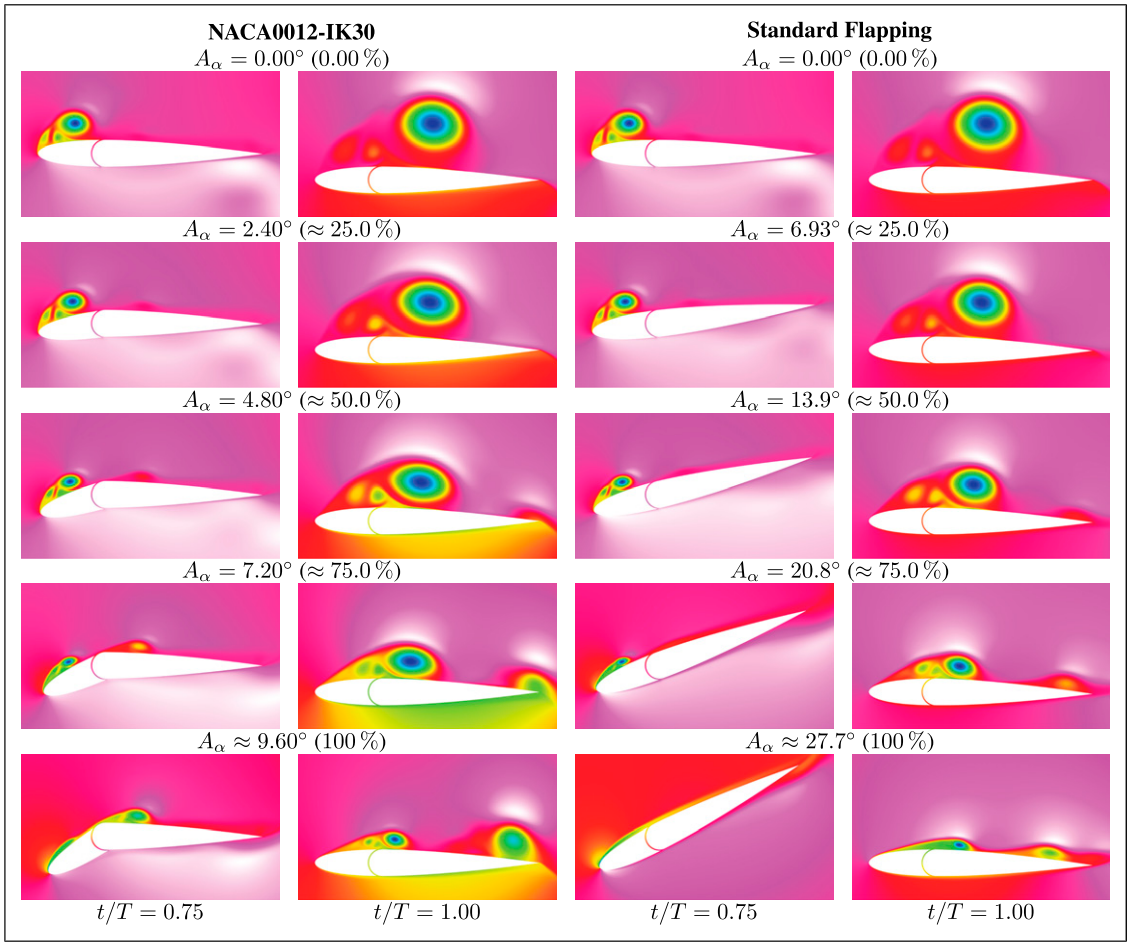

Figure 19. Optimization progress with φ = 0.0.

propulsive power, efficiency does not increase continuously with kh.

While standard flapping offers better efficiency, the NACA0012-IK30 mechanism offers a unique feature. The pitching amplitude that maximizes the mean propulsive power also offers near-optimal propulsive efficiency, making this a central outcome of the present study. The justification for such a feature is the fact that the power consumed by proposed flapping does not change as much as standard flapping with the leading edge pitching amplitude. This means that if $\overline{C_{P_R}}$ is kept fairly constant, when we maximize for $\overline{C_{P_P}}$ we will be finding also an efficiency maximum, as one can see by the propulsive efficiency definition. This is not achievable with conventional flapping airfoils. On the one hand, plunging airfoils present good thrust production, but propulsive efficiency

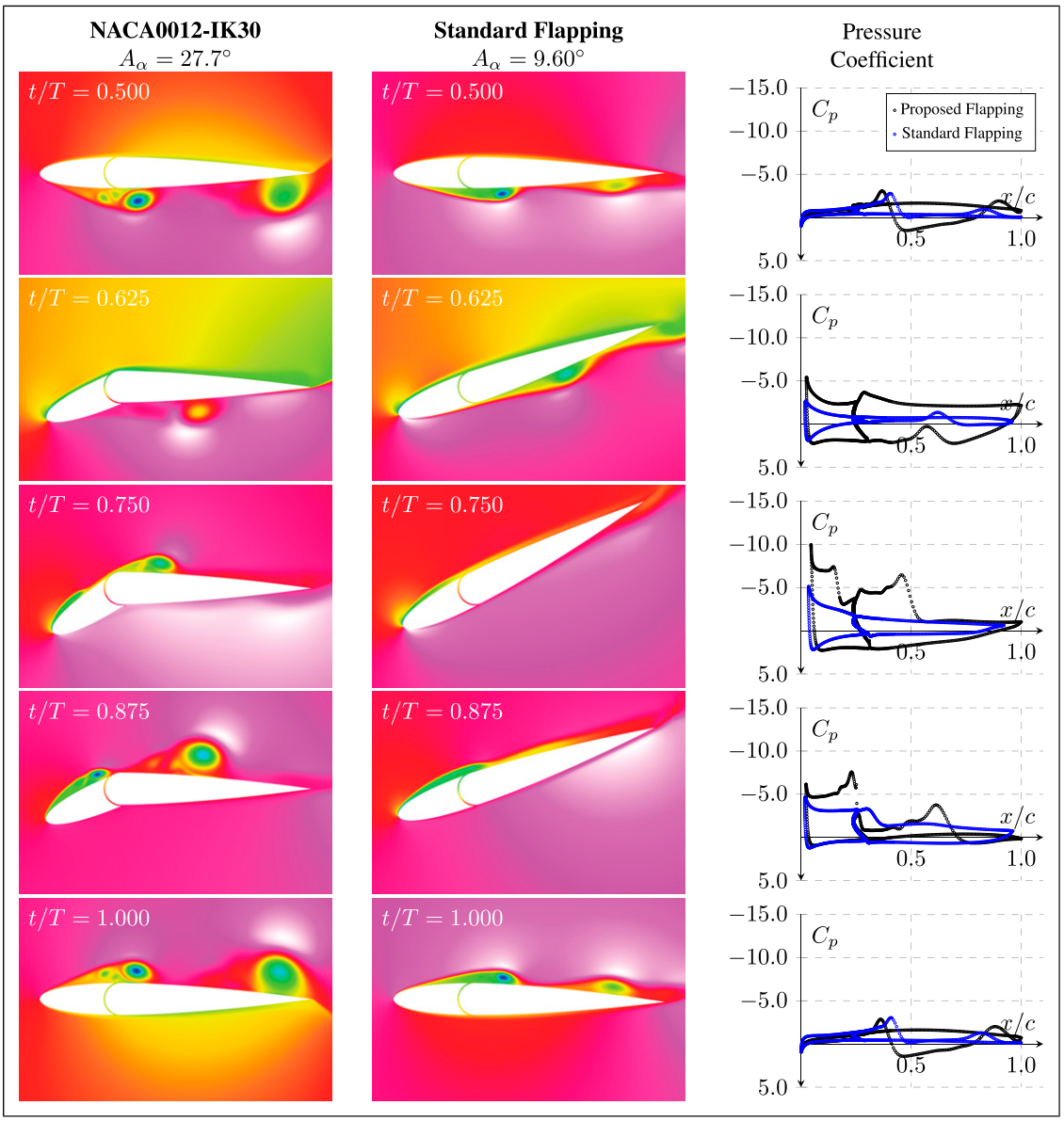

Figure 20. Pressure distribution for the two flapping modes at maximum propulsive efficiency (φ = 0.0).

typically takes a hit, while on the other hand, flapping, where plunging and pitching are combined, offers better efficiency at the expense of lower thrust.[6]

Figure 18 shows the efficiency as a function of the mean propulsive power. In standard flapping, the airfoil passes through maximum thrust generation, sacrificing it to reach optimal efficiency, as one can see by the curved paths created during optimization. In contrast, the proposed airfoil reaches optimal propulsive efficiency following a linear path in the $\overline{C_{P_p}}$ direction. Moreover, when we look at the same propulsive efficiency envelope, the -IK30 mechanism offers much-improved thrust performance, rendering standard flapping for these regimes impractical.

To supplement these graphs, Figure 19 shows the total pressure contour during the optimization progress of η, similar to what was shown for the mean propulsive power. An overall look at the snapshots leads to the primary conclusion that optimizing propulsive efficiency requires the nearly complete removal of the leading-edge vortex, regardless of flapping mode. This is verified halfway down ($t/T = 0.50$), where the LEV becomes smaller and smaller until its formation is minimal. Still, there is a suction zone that then separates and creates a slight separation region beyond the pivot point (t/T = 1.00).

In Figure 20, a closer view of the descent phase is given together with the pressure coefficient distribution for the two flapping modes. In the first half of the descent ($t/T = 0.625$), the flow on the upperside remains attached with the proposed flapping having two clear suction zones. These two regions then become separated (t/T = 0.75) judging by the interruption of the adverse pressure gradient seen at t/T = 0.625. In contrast, conventional flapping still has the flow attached but not for long since at t/T = 0.875, its adverse pressure gradient is also affected. The pressure distribution graphs reaffirm that the proposed geometry can provide more thrust while consuming more power.

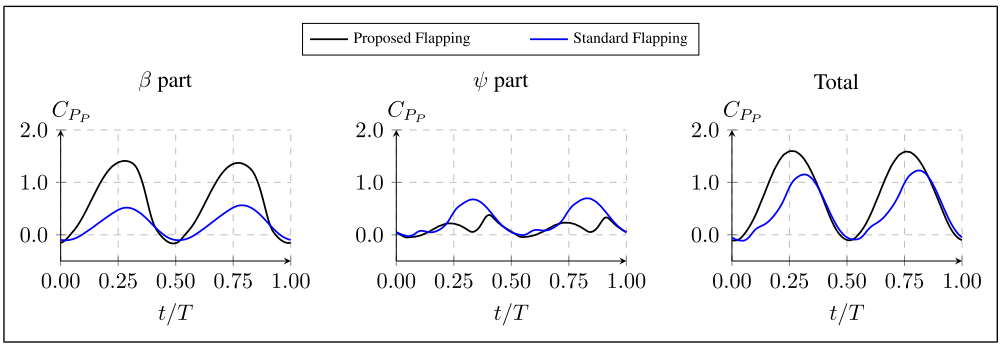

Figure 21. Propulsive power coefficient decomposition when φ = 0.0.

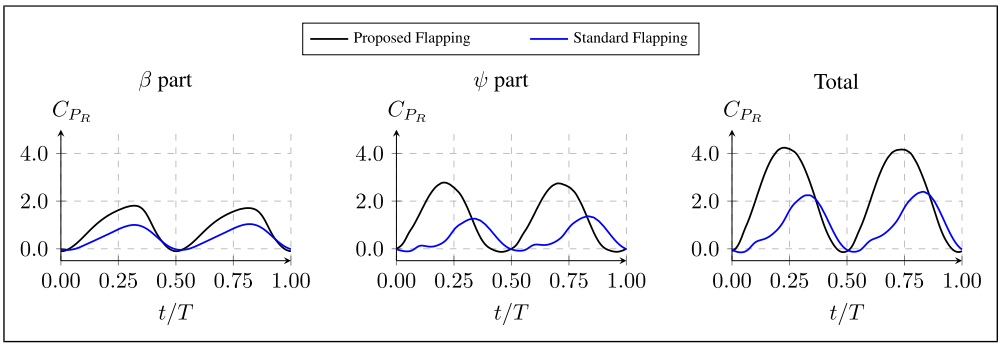

Figure 22. Required power coefficient decomposition when φ = 0.0.

This is corroborated by Figure 21, where the proposed flapping offers more propulsive power, with the major contributor being the β part. In contrast, thrust in conventional flapping is greatly influenced by the ψ part.

Though, as seen before, the higher thrust comes at the cost of higher power consumption. In fact, the proposed flapping can require two times more energy, as shown in Figure 22. However, as we saw in Figure 18, although conventional flapping achieves significant propulsive efficiencies with low power demand, it sacrifices the propulsive power to achieve it.

Conclusions

A newer flapping mode aimed at improving the propulsive performance is successfully achieved by modifying the NACA0012 airfoil. The proposed mechanism and standard flapping are compared parametrically and optimally at a Reynolds number of 10^4. The comparative framework is based on the equalization of kinematics, specifically, the effective angle of attack. Results show that the -IK30 mechanism offers higher propulsive power than standard flapping, although consuming more power. Its improvements become even more evident at higher nondimensional velocities. Thrust production and propulsive efficiency are optimized at the highest nondimensional amplitude using a weighted objective function. The proposed mechanism offers higher optimal thrust at a much lower pitching amplitude than standard flapping, though conventional flapping can reach higher propulsive efficiencies. However, the NACA0012-IK30 airfoil offers optimal thrust with near-optimal efficiency, something that is not achievable in traditional flapping airfoils, where they need to sacrifice one for another. The present work shows the flexibility of the proposed mechanism and the importance of the leading edge, and its impact on dynamically changing the airfoil geometry. Further research will be focused on studying different conditions, for instance, higher Reynolds numbers, and exploring the airfoil modification in different ways, especially the ψ part of the airfoil.

Declaration of conflicting interests

The author(s) declared no potential conflicts of interest with respect to the research, authorship, and/or publication of this article.

Funding

The author(s) disclosed receipt of the following financial support for the research, authorship, and/or publication of this article: This work was supported by the Foundation for Science and Technology (FCT) [grant numbers UIDB/50022/2020, UIDP/50022/2020, LA/P/0079/2020, 2020.04648.BD]; and the Brazilian National Council for Scientific and Technological Development [grant number #306824/2019-1].

ORCID iDs

Emanuel A.R. Camacho https://orcid.org/0000-0002-1648-8368
André R.R. Silva https://orcid.org/0000-0002-4901-7140

References

1. Shyy W, Aono H, kwon Kang C, et al. Introduction. In: *An introduction to flapping wing aerodynamics*. Cambridge,

MA: Cambridge University Press, 2013, pp. 1–41. DOI: 10.1017/cbo9781139583916.004.
2. Knoller R. Die gesetzedes luftwiderstandes. *Flug-und Motortechnik (Wien)* 1909; 3(21): 1–7.
3. Betz A. Ein beitrag zur erklaerung segelfluges. *Z Flugtech Motorluftschiffahrt* 1912; 3: 269–272.
4. von Kármán T and Burgers JM. *General aerodynamic theory - perfect fluids*. Berlin, Germany: Springer Berlin Heidelberg, 1935. DOI: 10.1007/978-3-642-91485-0.
5. Wu X, Zhang X, Tian X, et al. A review on fluid dynamics of flapping foils. *Ocean Eng* 2020; 195: 106712. DOI: 10.1016/j.oceaneng.2019.106712.
6. Gursul I and Cleaver D. Plunging oscillations of airfoils and wings: progress, opportunities, and challenges. *AIAA J* 2019; 57(9): 3648–3665. DOI: 10.2514/1.j056655.
7. Bao H, Yang W, Ma D, et al. Numerical simulation of flapping airfoil with alula. *Int J Micro Air Veh* 2020; 12: 175682932097798.
8. Lee S, Kim J, Park H, et al. The function of the Alula in Avian flight. *Sci Rep* 2015; 5(1): 9914–9915. DOI: 10.1038/srep09914.
9. Meseguer J, Franchini S, Pérez-Grande I, et al. On the aerodynamics of leading-edge high-lift devices of avian wings. *Proc Inst Mech Eng G J Aerosp Eng* 2005; 219(1): 63–68. DOI: 10.1243/095441005x9067.
10. Kim J, Park H, Jabłoński PG, et al. The function of the alula in avian flight. *Sci Rep* 2015; 5(1): 1–5.
11. Perry ML and Mueller TJ. Leading- and trailing-edge flaps on a low Reynolds number airfoil. *J Aircraft* 1987; 24(9): 653–659. DOI: 10.2514/3.45491.
12. Al-Garni AZ, Al-Garni AM, Ahmed SA, et al. Flow control for an airfoil with leading-edge rotation: an experimental study. *J Aircraft* 2000; 37(4): 617–622.
13. Niu J, Lei J and Lu T. Numerical research on the effect of variable droop leading-edge on oscillating NACA 0012 airfoil dynamic stall. *Aero Sci Technol* 2018; 72: 476–485.
14. Liu K, Song B, Xue D, et al. Numerical study of the aerodynamic effects of bio-inspired leading-edge serrations on a heaving wing at a low Reynolds number. *Aero Sci Technol* 2022; 124: 107529.
15. Jaworski JW. Thrust and aerodynamic forces from an oscillating leading edge flap. *AIAA J* 2012; 50(12): 2928–2931. DOI: 10.2514/1.j051579.
16. Theodorsen T. *General theory of aerodynamic instability and the mechanism of flutter*. Boston, MA: NACA Technical Report, 1935.
17. Garrick IE. Propulsion of a flapping and oscillating airfoil. *Report National Advisory Committee for Aeronautics, NACA Report* 1936; 567: 419–427.
18. Geissler W and van der Wall BG. Dynamic stall control on flapping wing airfoils. *Aero Sci Technol* 2017; 62: 1–10.
19. Camacho EAR, Neves FMSP, Marques FD, et al. Effects of a dynamic leading edge on a plunging airfoil. In: *AIAA aviation 2021 forum*. Reston: AIAA, 2021.
20. Camacho EA, Marques FD, Silva AR, et al. Leading-edge parametric study of the NACA0012-IK30 airfoil. In: *AIAA aviation 2022 forum*. Reston: AIAA, 2022.
21. Tuncer IH and Kaya M. Optimization of flapping airfoils for maximum thrust and propulsive efficiency. *AIAA J* 2005; 43(11): 2329–2336.
22. Kaya M and Tuncer IH. Nonsinusoidal path optimization of a flapping airfoil. *AIAA J* 2007; 45(8): 2075–2082. DOI: 10.2514/1.29478.
23. Yu M, Wang Z and Hu H. High-fidelity optimization of flapping airfoils for maximum propulsive efficiency. In: *51st AIAA aerospace sciences meeting including the new horizons forum and aerospace exposition*. Reston: AIAA, 2013.
24. Culbreth M, Allaneau Y and Jameson A. High-Fidelity Optimization of Flapping Airfoils and Wings. In: *29th AIAA applied aerodynamics conference*. American Institute of Aeronautics and Astronautics. Reston: AIAA, 2011.
25. Soueid H, Guglielmini L, Airiau C, et al. Optimization of the motion of a flapping airfoil using sensitivity functions. *Computers & Fluids* 2009; 38(4): 861–874. DOI: 10.1016/j.compfluid.2008.09.012.
26. Kaya M, Tuncer IH, Jones KD, et al. Optimization of flapping motion parameters for two airfoils in a biplane configuration. *J Aircraft* 2009; 46(2): 583–592. DOI: 10.2514/1.38796.
27. Spedding GR, Hedenstrom AH, McArthur J, et al. The implications of low-speed fixed-wing aerofoil measurements on the analysis and performance of flapping bird wings. *J Exp Biol* 2008; 211(2): 215–223. DOI: 10.1242/jeb.007823.
28. Young J and Lai JCS. Mechanisms influencing the efficiency of oscillating airfoil propulsion. *AIAA J* 2007; 45(7): 1695–1702. DOI: 10.2514/1.27628.
29. Heathcote S, Wang Z and Gursul I. Effect of spanwise flexibility on flapping wing propulsion. *J Fluid Struct* 2008; 24(2): 183–199. DOI: 10.1016/j.jfluidstructs.2007.08.003.
30. Barzilai J and Borwein JM. Two-point step size gradient methods. *IMA J Numer Anal* 1988; 8(1): 141–148. DOI: 10.1093/imanum/8.1.141.